

Tunable coupling of widely separated superconducting qubits: A possible application towards a modular quantum device

Peng Zhao,^{1,*} Yingshan Zhang,^{1,†} Guangming Xue,^{1,‡} Yirong Jin,¹ and Haifeng Yu¹

¹*Beijing Academy of Quantum Information Sciences, Beijing 100193, China*

(Dated: April 28, 2022)

Besides striving to assemble more and more qubits in a single monolithic quantum device, taking a modular design strategy may mitigate numerous engineering challenges for achieving large-scalable quantum processors with superconducting qubits. Nevertheless, a major challenge in the modular quantum device is how to realize high-fidelity entanglement operations on qubits housed in different modules while preserving the desired isolation between modules. In this brief note, we propose a conceptual design of a modular quantum device, where nearby modules are spatially separated by centimeters. In principle, each module can contain tens of superconducting qubits, and can be separately fabricated, characterized, packaged, and replaced. By introducing a bridge module between nearby qubit modules and taking coupling scheme utilizing tunable bus (a simple extension of the coupling scheme recently proposed in arXiv:2110.12570), tunable coupling of qubits that are housed in nearby qubit modules, could be realized. Given physically reasonable assumptions, we expect that sub-100-ns two-qubit gates for qubits housed in nearby modules which are spatially separated by more than two centimeters could be obtained. The inter-module gate operations are promising to be implemented with gate performance comparable with that of intra-module gate operations. The aim of this brief note is to show the possibility of solving challenges towards large-scale quantum devices, and to encourage further research in incorporating long-range inter-qubit coupling into scalable quantum information processing with superconducting qubits.

I. INTRODUCTION

After sustained and intense effort in the improvement of qubit performance and functionality, quantum devices with tens of superconducting qubits have been realized. This has led to impressive achievements in superconducting quantum-information processing [1–3]. Nevertheless, the current small-scale noisy quantum processor is still insufficient to support the pursuit of quantum advantage (e.g., solving complex problems that are intractable for classical computing) for practical applications [4] and the long-term goal of fault-tolerant quantum computing [5, 6]. Thus, in addition to striving for further improvement of qubit performance, focus also begins to shift to the scaling of these small-scale quantum devices into large-scale quantum systems. Integrating an increasing number of qubits without sacrificing qubit performance, especially in monolithic quantum devices, requires overcoming several scientific and technical challenges, such as wiring problem [7–9], crosstalk [10–12], and fabrication yield [13, 14]. To overcome these limitations, various schemes have been proposed and demonstrated, such as the compact integration of superconducting quantum devices with the classical cryogenic control systems [15–19], the three-dimensional (3D) integration technologies [20–25], and the post-processing of the fabricated qubit devices [26–28].

From a system integration perspective, building large quantum systems out of smaller modules may mitigate various challenges faced by monolithic integration strategy [17, 29–32]. As in modular quantum devices incorporating several modules, each module can be separately fabricated, charac-

terized, and replaced. Thus, the fabrication yield of the large modular system can be improved, and the electromagnetic crosstalk or impact of some correlated errors, such as caused by the high energy background radiation [33–35], may be restricted to the module scale. In addition, for modular quantum devices with larger spatial separation between modules, the vacant space between modules could be employed to increase the control footprint area for qubit control, and could even be used to integrate on-chip control electronics [15, 17, 19, 36]. This allows for a more-compact integration of the qubit device and its classical control system, thus potentially mitigating the wiring problem [7, 8]. Despite these appealing features, there is a major challenge in modular quantum devices, i.e., how to realize fast-speed, high-fidelity entanglement operations across qubits housed in different modules while keeping adequate isolation between modules (e.g., resulting in widely separated modules, thus each module can be processed individually).

In principle, qubits in the outer perimeter of each module device (e.g., the outermost qubits of a planar qubit device) can be directly coupled together. Therefore, inter-module gate operations can be implemented with performance comparable with that of the intra-module gate operation [32]. However, to ensure high-fidelity gate operations in multi-qubit systems, in general, qubits are coupled via a coupler circuit [37–40], which is employed to mitigate various quantum crosstalks. In this way, the entanglement gate operations are generally implemented with short-ranged coupling, limiting the spatial distance between coupled qubits to a few millimeters. Thus, in an ideal modular quantum device, this short-ranged coupling between inter-module qubits is not compatible with the desired isolation between modules.

In this note, we propose a conceptual design of a modular quantum device, where nearby qubit modules are spatially separated by centimeters. The inter-module qubits are tunably coupled via a bridge module. Thus, this can be employed for

*Electronic address: shangniguo@sina.com

†Electronic address: zhangys@baqis.ac.cn

‡Electronic address: xuegm@baqis.ac.cn

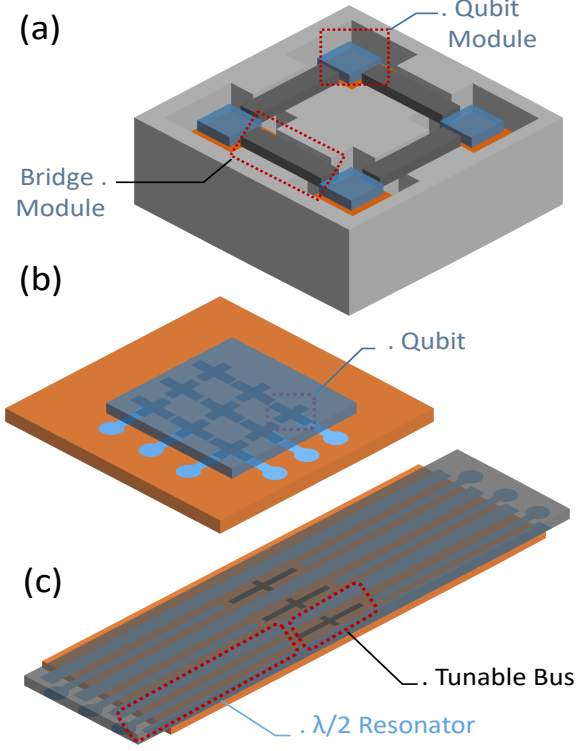


FIG. 1: Conceptual schematic of a possible modular quantum device utilizing bump bonding technologies (not to scale). (a) The modular quantum device comprises two types of functional modules: qubit modules and bridge modules. In principle, prior to assembly, each module can be separately fabricated, packaged, and characterized. After chip assembly and test, damaged modules resulting from ageing of qubit devices can also be replaced. (b) Same as the traditional monolithic quantum devices, each qubit module can contain tens of qubits and their ancillary circuits for qubit operations. As an example, the plot presented here shows that each qubit module contains a 3×3 qubit lattice, utilizing bump bonding technologies. (c) The bridge modules are introduced to mediate coupling between qubits that reside in nearby qubit modules, thus allowing for intra-module entanglement gate operations. The plot presented here shows that each bridge module comprises three coupler circuits, which are used to mediate inter-qubit coupling between qubits external to each qubit module. The coupler circuit, which has a sandwich coupling structure, consists of a half-wave superconducting coplanar waveguide resonator (i.e., $\lambda/2$ CPW resonator), one frequency-tunable transmon qubit [42] (used as the tunable bus), and another superconducting $\lambda/2$ CPW resonator.

implementing sub-100-ns Controlled-Z (CZ) gates for qubits housed in nearby qubit modules. This inter-module coupling scheme is a natural extension of a previously proposed coupling scheme utilizing a tunable bus [41]. Given physical assumptions, we expect that tunable coupling (entanglement gate operations) of qubits housed in nearby qubit modules that are spatially separated by more than two centimeters could be obtained.

II. OVERVIEW OF A MODULAR SUPERCONDUCTING QUANTUM PROCESSOR

As sketched in Fig. 1, we consider a modular quantum device comprising two types of functional modules: qubit modules and bridge modules. In principle, prior to the device assembly, each module can be separately fabricated, packaged, and characterized. Therefore, only the modules which function properly during the test, are assembled into the modular quantum device. After device assembly, damaged modules, such as due to the aging of qubit devices, can also be replaced with minimal impact on the performance of other functional modules.

In principle, same as the traditional monolithic quantum devices, each qubit module can contain tens of qubits and their ancillary circuits for qubit operations, e.g., readout resonators for qubit measurement, and qubit control lines for gate operations. The bridge modules are introduced to mediate coupling between qubits that reside in nearby qubit modules, thus allowing for inter-module entanglement gate operations. In this way, it is promising to scale up the quantum device without any sacrifice of connectivity of qubits. In addition, the bridge module can be introduced to decrease qubit density and create vacant space, which can increase the control footprint area for qubit control, thus potentially mitigating the wire problem [36].

As the surface code scheme requires a two-dimensional (2D) lattice of qubits with only nearest-neighbor interactions [5], here, only qubits in the outer perimeter of each module device need to be coupled to each other through the bridge modules. For the intra-module coupled qubits, we consider a simple extension of the coupling scheme recently proposed in Ref.[41], which shows that tunable ZZ coupling between two transmon qubits can be achieved through a tunable bus. The key potential benefit from this coupling scheme is that only rather weak qubit-bus coupling, typically with a strength of 20 MHz, is needed for implementing sub-100 ns CZ gates.

In the original protocol, the qubit and the tunable bus are coupled directly (via a coupled capacitor), thus limiting the spatial distance between coupled qubits to a few millimeters. Here, as sketched in Fig. 1(c), we consider that the qubit and the tunable bus are coupled via a half-wave superconducting coplanar waveguide resonator ($\lambda/2$ CPW resonator) [43, 44]. In this setup, a resonator-mediated longer-range qubit-bus coupling with the strength of around 20 MHz can be achieved [44]. Therefore, here, qubits that are widely spatial-separated can be coupled tunably. Given this longer-range coupling scheme, we expect that the modular quantum devices with large intra-module separation distance could be achieved, thus allowing for having the desired physical isolation between qubit modules.

III. ENTANGLEMENT OPERATIONS ON QUBITS HOUSED IN NEARBY MODULES

As sketched in Fig. 1(c), in the bridge module, a coupler circuit is introduced to mediate a tunable ZZ coupling be-

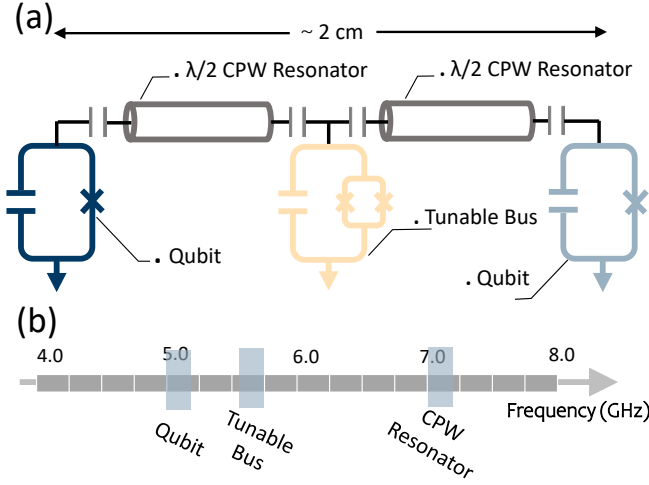


FIG. 2: Circuit schematic of the proposed coupling circuit for coupling qubits in nearby qubit modules (not to scale). (a) Two fixed-frequency transmon qubits that are spatially separated by 2 cm are coupled together via a coupler circuit. The circuit has a sandwich structure, and consists of a $\lambda/2$ resonator, a frequency-tunable transmon qubit (acted as the tunable bus), and another $\lambda/2$ CPW resonator. (b) Frequency arrangement of the qubit and the coupler circuit (two $\lambda/2$ CPW resonators and one tunable bus). The qubit frequency is around 5.0 GHz, the tunable-bus frequency is typically above 500 MHz of the qubit's, and the fundamental mode frequency of the resonator is about 7.0 GHz.

tween the qubits external to nearby qubit modules. The circuit has a sandwich structure, and consists of a $\lambda/2$ CPW resonator, one frequency-tunable transmon qubit (acted as a tunable bus), and another $\lambda/2$ CPW resonator. In the following discussion, we give a detailed analysis of this coupling circuit.

Figure 2(a) shows the circuit schematic of a coupled two-qubit system, where two fixed-frequency transmon qubits (housed in the nearby qubit modules) are coupled via a coupler circuit (housed in the bridge module). The full coupled system can be modeled by a chain of five modes (including three anharmonic modes, i.e., two qubits and one tunable bus, and two harmonic modes, i.e., two $\lambda/2$ CPW resonators) with nearest-neighboring coupling, described by (hereafter $\hbar = 1$)

$$\begin{aligned}
 H = & \sum_{i=1,2,t} \left(\omega_i a_i^\dagger a_i + \frac{\eta_i}{2} a_i^\dagger a_i^\dagger a_i a_i \right) + \sum_{j=1,2} \omega_{rj} b_j^\dagger b_j \\
 & + \sum_{k=1,2} g_{tk} (a_t^\dagger + a_t)(b_k + b_k^\dagger) \\
 & + \sum_{k=1,2} g_{rk} (a_k^\dagger + a_k)(b_k + b_k^\dagger),
 \end{aligned} \quad (1)$$

where the subscript $i = \{1, 2, t\}$ labels the anharmonic mode Q_i with anharmonicity η_i and bare mode frequency ω_i , and the subscript $j = \{1, 2\}$ labels the harmonic mode R_j with bare mode frequency ω_{rj} . a_i (a_i^\dagger) is the annihilation (creation) operator for the anharmonic modes Q_i , and b_j (b_j^\dagger) is for harmonic modes R_j . g_{tk} (g_{rk}) denotes the coupling strength between the tunable bus Q_t (the qubit Q_k) and the resonator R_k .

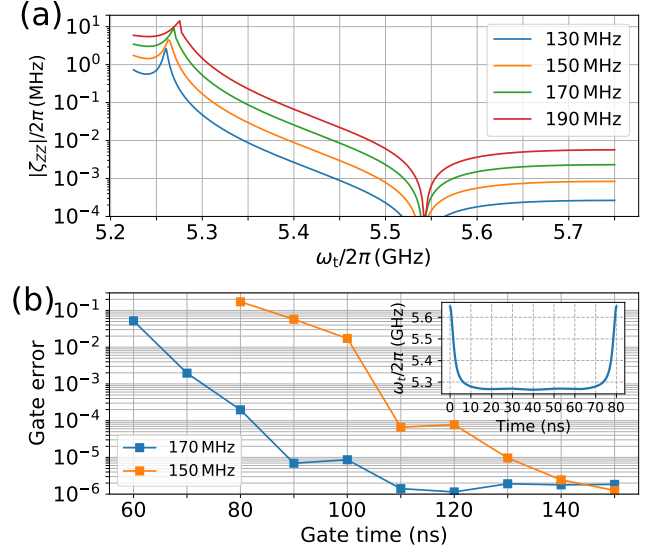


FIG. 3: Tunable ZZ coupling and its application for implementing two-qubit CZ gates. (a) ZZ coupling strength ζ_{zz} as a function of the bus frequency ω_t for the coupled qubit system illustrated in Fig. 2(a) with qubit frequency $\omega_{1(2)}/2\pi = 5.0(5.2)$ GHz, qubit (bus) anharmonicity $\eta_1 = \eta_2 = \eta_t = \eta$ ($\eta/2\pi = -300$ MHz), resonator frequency $\omega_{r1(r2)}/2\pi = 7.0(7.2)$ GHz, and qubit (bus)-resonator coupling strength $g_{tk} = g_{rk} = g$ (calculated at $\omega_i/2\pi = \omega_{rj}/2\pi = 6.0$ GHz). Here we consider the coupling strength $g/2\pi = \{130, 150, 170, 190\}$ MHz. (b) Intrinsic two-qubit CZ gate errors versus gate time with $g/2\pi = \{150, 170\}$ MHz (without the consideration of system decoherence process). Here the idle frequency of the tunable bus is set at 5.65 GHz, where the residual ZZ coupling is suppressed below 10 kHz, as shown in (a), the other system parameters are the same as in (a). The inset shows the typical control pulse shape of the bus frequency ω_t during the implementation of the CZ gate.

As shown in Fig. 2(b), here we consider that the qubit frequency is around 5.0 GHz, the tunable-bus frequency is typically above 500 MHz of the qubit's, and the resonator frequency is about 7.0 GHz. Assuming that the dielectric constant of the substrate (silicon) to be $\epsilon_r = 11.45$, the superconducting $\lambda/2$ CPW resonator with the length 9 mm has the fundamental mode at 7 GHz [45, 46]. As the typical size of the transmon qubit or the tunable bus (i.e., a frequency-tunable transmon qubit) is about 1 mm [9], we expect that coupling of qubits that are spatially separated by more than 2 cm can be realized. Furthermore, as illustrated in the previous work [41], in this setup, the ZZ coupling of qubits can be controlled by adjusting the frequency of the tunable bus. Thus, two-qubit CZ gates can be realized when turning on the ZZ coupling, while residual ZZ coupling can be suppressed heavily when turning off this coupling.

As shown in Fig. 3(a), we show the ZZ coupling between the two qubits versus the frequency of the tunable bus with different qubit-bus and bus-resonator coupling strength $g/2\pi \in \{130, 150, 170, 190\}$ MHz. Here, the ZZ coupling

strength is defined as

$$\zeta_{ZZ} \equiv (E_{11} - E_{10}) - (E_{01} - E_{00}), \quad (2)$$

and can be obtained numerically by diagonalizing the full system Hamiltonian in Eq. (1). In Eq. (2), E_{jk} denotes eigenenergy of the full system associated with dressed eigenstate $|\tilde{j}k\rangle$, which is adiabatically connected to the bare state $|j000k\rangle$ (here notation $|Q_1 R_1 Q_t R_2 Q_2\rangle$ is used, denoting the system state). One can find that when qubit (bus)-resonator coupling strength g take values large than 170 MHz, ZZ coupling with the strength around 10 MHz can be achieved. As illustrated in Ref.[41], this tunable ZZ coupling can be used to realize sub-100 ns CZ gates. In addition, during the system idle point (for single-qubit gate operations), the ZZ coupling can also be suppressed below 10 kHz when turning off the coupling.

To evaluate the gate performance in the proposed coupling scheme, Figure 3(b) shows the two-qubit CZ gate error as a function of the gate time without the consideration of the system decoherence process [47]. Here, the CZ gate is implemented by tuning the frequency of the tunable bus according to a fast adiabatic control pulse [48], and the typical control pulse shape of the bus frequency can be found in the inset of Fig. 3(b). The detailed procedure for tuning up the fast-adiabatic CZ gate and characterizing the intrinsic CZ gate performance (i.e., without the consideration of decoherence process) is the same as in Ref.[41]. One can find that with the qubit (bus)-resonator coupling strength of 170 MHz, high-fidelity sub-100 ns CZ gates can be achieved. In addition, while two addition resonators are employed in the present gate scheme, the gate performance is comparable to those in the original scheme [41], which relies on short-ranged coupling, thus favoring intra-module gate operations. This suggests that with this simple tunable coupling scheme, the inter-module gate operations are promising to be implemented with gate performance comparable with that of intra-module gate operations.

In practical implementations, compared with the original coupling scheme, one may expect that besides the decoherence processes of the two qubits and the tunable bus, the difficulties to face with the present scheme depend on one additional limitation, i.e., the resonator decay process. Here, to study the influence of the resonator decay process on the CZ gate performance, the Lindblad master equation is employed. To be more specific, by considering the resonator decay process, the master equation can be expressed as

$$\frac{d\rho}{dt} = -i[H, \rho] + \sum_{j=1,2} \kappa_j \mathcal{L}[b_j], \quad (3)$$

where the Hamiltonian H is given in Eq. (1), ρ is the reduced density matrix of the system, $\mathcal{L}[b_j] = b_j \rho b_j^\dagger - b_j^\dagger b_j \rho / 2 - \rho b_j^\dagger b_j / 2$ describes the resonator decay terms, κ_j denotes the photon decay rate of resonator R_j . The average gate fidelity of the CZ gate under resonator decay process is defined as [49]

$$F = \frac{d F_p + 1 - L_1}{d + 1}, \quad (4)$$

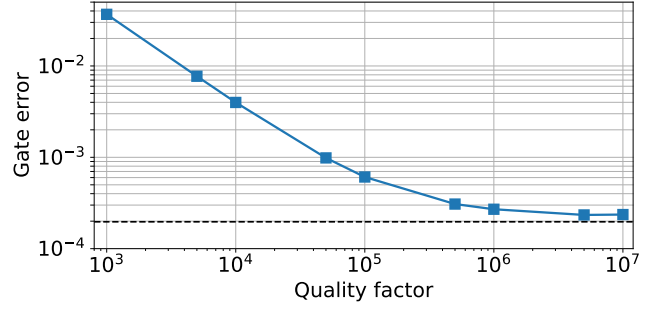


FIG. 4: CZ gate error versus the quality factor (Q) of the $\lambda/2$ CPW resonator. Here the gate time is 80 ns, qubit (bus)-resonator coupling strength is $g/2\pi = 170$ MHz, and the quality factors of the two resonators take the same value ($Q_1 = Q_2 = Q$). The decay rates of the two resonators are $\kappa_1 = \omega_{r1}/Q$ and $\kappa_2 = \omega_{r2}/Q$. The other system parameters are the same as in Fig. 3. The black dashed line denotes the gate error without the consideration of the resonator decay process, i.e., $\kappa_1 = \kappa_2 = 0$.

where d denotes the dimension of the computational subspace of the system, L_1 represents the leakage of the gate operation, and F_p is the process fidelity of the implemented CZ gate. The process fidelity F_p can be obtained by numerically performing quantum process tomography of the implemented CZ gate based on the master equation given in Eq. (3). Similarly, the leakage L_1 can be obtained by solving the master equation with the system initialized in different computational states [49].

Figure 4 shows the CZ gate error $1 - F$ versus the quality factor (Q) of the resonator. One can find that CZ gate errors below 0.01 (0.001) can be achieved with the resonator quality factor exceeding 5×10^3 (5×10^4). Given the state-of-the-art results, planar superconducting CPW resonators with internal quality factors above 10^6 have been demonstrated [50–52]. Therefore, the result shown in Fig. 4 suggests that with current technologies, the gate error from the resonator decay process is promising to be pushed below 0.001.

Overall, from the above discussion, the longer-range tunable coupling scheme is promising to realize a modular quantum device with high-fidelity entanglement gate operations among modules and to achieve a desired physical isolation between qubit modules.

IV. DISCUSSION AND CONCLUSION

In summary, this brief note aims to show the possibility of solving challenges towards large-scale quantum devices with tunable longer-range coupling. We have shown that with the proposed tunable longer-range coupling, a modular quantum device with fast-speed, high-fidelity inter-module gate operations and desired physical isolation could be obtainable. This could give rise to a promising foundation for mitigating several scientific and technical challenges towards large-scale superconducting quantum computing. While, in practice, the

feasibility of the proposed modular design may be limited because of several relevant engineering challenges, e.g., the assembly accuracy of modules [32], and the parasitic electromagnetic modes within the device package [10, 12], another goal of this note is to encourage further experimental and theoretical research in incorporating long-range inter-qubit coupling into scalable quantum information processing with superconducting qubits [53].

Acknowledgments

We would like to thank Xuegang Li and Junling Long for their helpful discussions and comments. Numerical analysis of the resonator decay process on gate performance were performed using the Quantum Toolbox in Python (QuTiP) [54].

-
- [1] F. Arute, K. Arya, R. Babbush, D. Bacon, J. C. Bardin, R. Barends, R. Biswas, S. Boixo, F. G. Brandao, D. A. Buell *et al.*, Quantum supremacy using a programmable superconducting processor, *Nature* **574**, 505 (2019).
 - [2] Q. Zhu, S. Cao, F. Chen, M.-C. Chen, X. Chen, T.-H. Chung, H. Deng, Y. Du, D. Fan, M. Gong *et al.*, Quantum computational advantage via 60-qubit 24-cycle random circuit sampling, *Science Bulletin* **67**, 240 (2022).
 - [3] P. Jurcevic, A. Javadi-Abhari, L. S. Bishop, I. Lauer, D. F. Bogorin, M. Brink, L. Capelluto, O. Günlük, T. Itoko, N. Kanazawa *et al.*, Demonstration of quantum volume 64 on a superconducting quantum computing system, *Quantum Sci. Technol.* **6**, 025020 (2021).
 - [4] J. Preskill, Quantum Computing in the NISQ era and beyond, *Quantum* **2**, 79 (2018).
 - [5] A. G. Fowler, M. Mariantoni, J. M. Martinis, and A. N. Cleland, Surface codes: Towards practical large-scale quantum computation, *Phys. Rev. A* **86**, 032324 (2012).
 - [6] J. M. Martinis, Qubit Metrology for Building a Fault Tolerant Quantum Computer, *npj Quantum Inf.* **1**, 15005 (2015).
 - [7] D. P. Franke, J. S. Clarke, L. M. K. Vandersypen, and M. Veldhorst, Rent's rule and extensibility in quantum computing, *Microprocess. Microsy.* **67**, 1 (2019).
 - [8] D. J. Reilly, Challenges in Scaling-up the Control Interface of a Quantum Computer, *2019 IEEE International Electron Devices Meeting (IEDM)*, 31.7 (2019).
 - [9] J. M. Martinis, Information Constraints for Scalable Control in a Quantum Computer, *arXiv:2012.14270*.
 - [10] J. Wenner, M. Neeley, R. C. Bialczak, M. Lenander, E. Lucero, A. D. O'Connell, D. Sank, H. Wang, M. Weides, A. N. Cleland, and J. M. Martinis, Wirebond cross talk and cavity modes in large chip mounts for superconducting qubits, *Supercond. Sci. Technol.* **24**, 065001 (2011).
 - [11] R. Barends, J. Kelly, A. Megrant, A. Veitia, D. Sank, E. Jeffrey, T. C. White, J. Mutus, A. G. Fowler, B. Campbell *et al.*, Superconducting quantum circuits at the surface code threshold for fault tolerance, *Nature* **508**, 500 (2014).
 - [12] S. Huang, B. Lienhard, G. Calusine, A. Vepsäläinen, J. Braumüller, D. K. Kim, A. J. Melville, B. M. Niedzielski, J. L. Yoder, B. Kannan *et al.*, Microwave Package Design for Superconducting Quantum Processors, *PRX Quantum* **2**, 020306 (2021).
 - [13] J. M. Gambetta, J. M. Chow, and M. Steffen, Building logical qubits in a superconducting quantum computing system, *npj Quantum Inf.* **3**, 2 (2017).
 - [14] M. Brink, J. M. Chow, J. Hertzberg, E. Magesan, and Sami Rosenblatt, Device challenges for near term superconducting quantum processors: frequency collisions, *2018 IEEE International Electron Devices Meeting (IEDM)*, (2018).
 - [15] E. Leonard Jr., M. A. Beck, J. Nelson, B.G. Christensen, T. Thorbeck, C. Howington, A. Opremcak, I.V. Pechenezhskiy, K. Dodge, N.P. Dupuis *et al.*, Digital Coherent Control of a Superconducting Qubit, *Phys. Rev. Appl.* **11**, 014009 (2019).
 - [16] R. McDermott, M. G. Vavilov, B. L. T. Plourde, F. K. Wilhelm, P. J. Liebermann, O. A. Mukhanov and T. A. Ohki, Quantum-classical interface based on single flux quantum digital logic, *Quantum Sci. Technol.* **3**, 024004 (2018).
 - [17] R. N. Das, J. L. Yoder, D. Rosenberg, D. K. Kim, D. Yost, J. Mallek, D. Hover, V. Bolkhovsky, A. J. Kerman, and W. D. Oliver, Cryogenic qubit integration for quantum computing, *2018 IEEE 68th Electronic Components and Technology Conference (ECTC)*, 504 (2018).
 - [18] J. C. Bardin, E. Jeffrey, E. Lucero, T. Huang, S. Das, D. T. Sank, O. Naaman, A. E. Megrant, R. Barends, T. White *et al.*, Design and Characterization of a 28-nm Bulk-CMOS Cryogenic Quantum Controller Dissipating Less Than 2 mW at 3 K, *IEEE Journal of Solid-State Circuits* **54**, 3043 (2019).
 - [19] A. Potočnik, S. Brebels, J. Verjauw, R. Acharya, A. Grill, D. Wan, M. Mongillo, R. Li, T. Ivanov, S. V. Winckel *et al.*, Millikelvin temperature cryo-CMOS multiplexer for scalable quantum device characterisation, *Quantum Sci. Technol.* **7**, 015004 (2021).
 - [20] J. H. Béjanin, T. G. McConkey, J. R. Rinehart, C. T. Earnest, C. R. H. McRae, D. Shiri, J. D. Bateman, Y. Rohanizadeh, B. Penava, P. Breul *et al.*, Three-Dimensional Wiring for Extensible Quantum Computing: The Quantum Socket, *Phys. Rev. Appl.* **6**, 044010 (2016).
 - [21] Q. Liu, M. Li, K. Dai, K. Zhang, G. Xue, X. Tan, H. Yu, and Y. Yu, Extensible 3D architecture for superconducting quantum computing, *Appl. Phys. Lett.* **110**, 232602 (2017).
 - [22] D. Rosenberg, D. Kim, R. Das, D. Yost, S. Gustavsson, D. Hover, P. Krantz, A. Melville, L. Racz, G. O. Samach *et al.*, 3D integrated superconducting qubits, *npj Quantum Inf.* **3**, 1 (2017).
 - [23] N. T. Bronn, V. P. Adiga, S. B. Olivadese, X. Wu, J. M. Chow, and D. P. Pappas, High coherence plane breaking packaging for superconducting qubits, *Quantum Sci. Technol.* **3**, 024007 (2018).
 - [24] B. Foxen, J. Y. Mutus, E. Lucero, R. Graff, A. Megrant, Y. Chen, C. Quintana, B. Burkett, J. Kelly, E. Jeffrey *et al.*, Qubit compatible superconducting interconnects, *Quantum Sci. Technol.* **3**, 014005 (2018).
 - [25] P. A. Spring, T. Tsunoda, B. Vlastakis, and P. J. Leek, Modeling Enclosures for Large-Scale Superconducting Quantum Circuits, *Phys. Rev. Appl.* **14**, 024061 (2020).
 - [26] C. Granata, A. Vettoliere, L. Petti, M. Rippa, B. Ruggiero, P. Mornile, and M. Russo, Trimming of critical current in niobium Josephson devices by laser annealing, *J. Phys. Conf. Ser.* **97**, 012110 (2008).
 - [27] J. B. Hertzberg, E. J. Zhang, S. Rosenblatt, E. Magesan, J. A. Smolin, J.-B. Yau, V. P. Adiga, M. Sandberg, M. Brink, J. E. M. Chow, and J. S. Orcutt, Laser-annealing Josephson junctions for yielding scaled-up superconducting quantum processes

- sors, *npj Quantum Inf.* **7**, 129 (2021).
- [28] M. Mergenthaler, C. Müller, M. Ganzhorn, S. Paredes, P. Müller, G. Salis, V.P. Adiga, M. Brink, M. Sandberg, J.B. Hertzberg, S. Filipp, and A. Fuhrer, Effects of surface treatments on flux tunable transmon qubits, *npj Quantum Inf.* **7**, 157 (2021).
- [29] T. Brecht, W. Pfaff, C. Wang, Y. Chu, L. Frunzio, M. H. Devoret, and R. J. Schoelkopf, Multilayer microwave integrated quantum circuits for scalable quantum computing, *npj Quantum Inf.* **2**, 1 (2016).
- [30] C. Axline, M. Reagor, R. Heeres, P. Reinhold, C. Wang, K. Shain, W. Pfaff, Y. Chu, L. Frunzio, and R. J. Schoelkopf, An architecture for integrating planar and 3D cQED devices, *Appl. Phys. Lett.* **109**, 042601 (2016).
- [31] C. Zhou, P. Lu, M. Praquin, T.-C. Chien, R. Kaufman, X. Cao, M. Xia, R. Mong, W. Pfaff, D. Pekker, and M. Hatridge, A modular quantum computer based on a quantum state router, *arXiv:2109.06848*.
- [32] A. Gold, J. P. Paquette, A. Stockklauser, M. J. Reagor, M. S. Alam, A. Bestwick, N. Didier, A. Nersisyan, F. Oruc, A. Razavi *et al.*, Entanglement across separate silicon dies in a modular superconducting qubit device, *npj Quantum Inf.* **7**, 142 (2021).
- [33] A. P. Vepsäläinen, A. H. Karamlou, J. L. Orrell, A. S. Dogra, B. Loer, F. Vasconcelos, D. K. Kim, A. J. Melville, B. M. Niedzielski, J. L. Yoder *et al.*, Correlated charge noise and relaxation errors in superconducting qubits, *Nature* **584**, 551 (2020).
- [34] C. D. Wilen, S. Abdullah, N. A. Kurinsky, C. Stanford, L. Cardani, G. D’Imperio, C. Tomei, L. Faoro, L. B. Ioffe, C. H. Liu *et al.*, Correlated charge noise and relaxation errors in superconducting qubits, *Nature* **594**, 369 (2021).
- [35] L. Cardani, F. Valenti, N. Casali, G. Catelani, T. Charpentier, M. Clemenza, I. Colantoni, A. Cruciani, G. D’Imperio, L. Gironi *et al.*, Reducing the impact of radioactivity on quantum circuits in a deep-underground facility, *Nat. Commun.* **12**, 2733 (2021).
- [36] J. M. Boter, J. P. Dehollain, J. P. G. van Dijk, Y. Xu, T. Hensgens, R. Versluis, H. W. L. Naus, J. S. Clarke, M. Veldhorst, F. Sebastiano, and L. M. K. Vandersypen, The spider-web array a sparse spin qubit array, *arXiv:2110.00189*.
- [37] Y. Chen, C. Neill, P. Roushan, N. Leung, M. Fang, R. Barends, J. Kelly, B. Campbell, Z. Chen, B. Chiaro *et al.*, Qubit architecture with high coherence and fast tunable coupling, *Phys. Rev. Lett.* **113**, 220502 (2014).
- [38] D. C. McKay, S. Filipp, A. Mezzacapo, E. Magesan, J. M. Chow, and J. M. Gambetta, Universal gate for fixed-frequency qubits via a tunable bus, *Phys. Rev. Appl.* **6**, 064007 (2016).
- [39] F. Yan, P. Krantz, Y. Sung, M. Kjaergaard, D. L. Campbell, T. P. Orlando, S. Gustavsson, and W. D. Oliver, Tunable Coupling Scheme for Implementing High-Fidelity Two-Qubit Gates, *Phys. Rev. Appl.* **10**, 054062 (2018).
- [40] P. S. Mundada, G. Zhang, T. Hazard, and A. A. Houck, Suppression of Qubit Crosstalk in a Tunable Coupling Superconducting Circuit, *Phys. Rev. Appl.* **12**, 054023 (2019).
- [41] P. Zhao, K. Linghu, Z. Li, P. Xu, R. Wang, G. Xue, Y. Jin, and H. Yu, Quantum Crosstalk Analysis for Simultaneous Gate Operations on Superconducting Qubits, *PRX Quantum* **3**, 020301 (2022).
- [42] J. Koch, T. M. Yu, J. Gambetta, A. A. Houck, D. I. Schuster, J. Majer, A. Blais, M. H. Devoret, S. M. Girvin, and R. J. Schoelkopf, Charge-insensitive qubit design derived from the cooper pair box, *Phys. Rev. A* **76**, 042319 (2007).
- [43] M. A. Sillanpää, J. I. Park, and R. W. Simmonds, Coherent quantum state storage and transfer between two phase qubits via a resonant cavity, *Nature (London)* **449**, 438 (2007).
- [44] J. Majer, J. M. Chow, J. M. Gambetta, J. Koch, B. R. Johnson, J. A. Schreier, L. Frunzio, D. I. Schuster, A. A. Houck, A. Wallraff *et al.*, Coupling superconducting qubits via a cavity bus, *Nature (London)* **449**, 443 (2007).
- [45] M. Göppl, A. Fragner, M. Baur, R. Bianchetti, S. Filipp, J. M. Fink, P. J. Leek, G. Puebla, L. Steffen, and A. Wallraff, Coplanar waveguide resonators for circuit quantum electrodynamics, *J. Appl. Phys.* **104**, 113904 (2008).
- [46] D. M. Pozar, *Microwave Engineering* (Wiley, 2011).
- [47] L. H. Pedersen, N. M. Møller, and K. Mølmer, Fidelity of quantum operations, *Phys. Lett. A* **367**, 47 (2007).
- [48] J. M. Martinis and M. R. Geller, Fast adiabatic qubit gates using only σ^z control, *Phys. Rev. A* **90**, 022307 (2014).
- [49] C. J. Wood and J. M. Gambetta, Quantification and characterization of leakage errors, *Phys. Rev. A* **97**, 032306 (2018).
- [50] A. Megrant, C. Neill, R. Barends, B. Chiaro, Y. Chen, L. Feigl, J. Kelly, Erik Lucero, M. Mariantoni, P. J. J. O’Malley *et al.*, Planar superconducting resonators with internal quality factors above one million, *Appl. Phys. Lett.* **100**, 113510 (2012).
- [51] G. Calusine, A. Melville, W. Woods, R. Das, C. Stull, V. Bolkhovsky, D. Braje, D. Hover, D. K. Kim, X. Milosshi *et al.*, Analysis and mitigation of interface losses in trench superconducting coplanar waveguide resonators, *Appl. Phys. Lett.* **112**, 062601 (2018).
- [52] R. Gao, W. Yu, H. Deng, H.-S. Ku, Z. Li, M. Wang, X. Miao, Y. Lin, and C. Deng, Epitaxial titanium nitride microwave resonators: Structural, chemical, electrical, and microwave properties, *Phys. Rev. Materials* **6**, 036202 (2022).
- [53] M. A. Tremblay, N. Delfosse, and M. E. Beverland, Constant-overhead quantum error correction with thin planar connectivity, *arXiv:2109.14609*.
- [54] J. Johansson, P. Nation, and F. Nori, QuTiP: An open-source Python framework for the dynamics of open quantum systems, *Comput. Phys. Commun.* **183**, 1760 (2012).